Photolabeling the *Torpedo* Nicotinic Acetylcholine Receptor with 4-Azido-2,3,5,6-tetrafluorobenzoylcholine, a Partial Agonist†

Selvanayagam Nirthanan, Michael R. Ziebell, David C. Chiara, Filbert Hong, and Jonathan B. Cohen*

Department of Neurobiology, Harvard Medical School, 220 Longwood Avenue, Boston, Massachusetts 02115

Received June 23, 2005; Revised Manuscript Received August 18, 2005

ABSTRACT: The interactions of a photoreactive analogue of benzoylcholine, 4-azido-2,3,5,6-tetrafluorobenzoylcholine (APFBzcholine), with nicotinic acetylcholine receptors (nAChRs) were studied using electrophysiology and photolabeling. APFBzcholine acted as a low-efficacy partial agonist, eliciting maximal responses that were 0.3 and 0.1% of that of acetylcholine for embryonic mouse and *Torpedo* nAChRs expressed in *Xenopus* oocytes, respectively. Equilibrium binding studies of [^{3}H]APFBzcholine with nAChR-rich membranes from *Torpedo* electric organ revealed equal affinities (K_{eq} = 12 μM) for the two agonist binding sites. Upon UV irradiation at 254 nm, [^{3}H]APFBzcholine was photoincorporated into the nAChR α, γ, and δ subunits in an agonist-inhibitable manner. Photolabeled amino acids in the agonist binding sites were identified by Edman degradation of isolated, labeled subunit fragments. [^{3}H]APFBzcholine photolabeled γLeu-109/δLeu-111, γTyr-111, and γTyr-117 in binding site segment E as well as αTyr-198 in α subunit binding site segment C. The observed pattern of photolabeling is examined in relation to the predicted orientation of the azide when APFBzcholine is docked in the agonist binding site of a homology model of the nAChR extracellular domain based upon the structure of the snail acetylcholine binding protein.

The *Torpedo* nicotinic acetylcholine receptor (nAChR)[1] is a representative member of a pharmacologically important superfamily of ligand-gated ion channels that includes the excitatory muscle and neuronal nAChRs and the serotonin $5HT_3$ receptor, as well as the inhibitory $GABA_A$ and glycine receptors. nAChRs from vertebrate skeletal muscle and the electric organs of *Torpedo* rays are heteropentamers of homologous subunits with a stoichiometry of 2α:β:γ(ϵ):δ that are arranged pseudosymmetrically around a central cation-selective ion channel (*1*, *2*). Each *Torpedo* nAChR contains two binding sites for acetylcholine (ACh) that are located in the extracellular domain at the α−γ and α−δ subunit interfaces, and the ion channel opens in response to agonist binding simultaneously to both sites. Affinity labeling and mutagenesis studies as well as the recent crystallographic structures of the snail ACh binding protein (AChBP), a homopentameric, secreted protein that is homologous to the nAChR extracellular domain, establish that the agonist binding sites are composed of aromatic and hydrophobic residues from three noncontiguous regions of the α subunit [binding-site segments A (α93), B (α149), and C (α190−200)] and by two or more regions of the γ(ϵ)/δ subunits [D (γ55−59) and E (γ109−119)] (*1*−*5*).

In the absence of high-resolution crystal structures of nAChRs complexed with agonists or antagonists, information about the mode of agonist binding as compared to antagonist can be obtained only from less direct methods. Analyses of the binding of the classic competitive antagonist *d*-tubocurarine (dTC) and its structural analogues to wild-type and mutant mouse and *Torpedo* nAChRs have established their likely orientation in the binding site (*6*, *7*) but also established that ligands of closely related structure can bind in different orientations (*8*). Mutational analyses established the importance of the core aromatics in the α subunit in agonist binding segments A−C as determinants of agonist gating and affinity (*3*), and the introduction of unnatural amino acids has revealed the importance of strong cation−π interactions between the indole side chain of αTrp-149 and the quaternary ammonium of ACh (*9*), but not for the positive charge of nicotine (*10*).

Photolabeling studies with [^{3}H]dTC and [^{3}H]nicotine provided direct evidence that agonists as well as antagonists were bound at subunit interfaces and identified amino acids in the γ/δ subunits as well as the α subunit that contribute to the binding sites (*11*, *12*), but with the structures of the

† This research was supported in part by United States Public Health Service Grant GM-58448 and by an award to Harvard Medical School from the Howard Hughes Medical Institute Biomedical Research Support Program. M.R.Z. was supported by Training Grant T32-NS07484, and S.N. was supported by a Brooks Foundation Research Fellowship in Neurobiology.

* To whom correspondence should be addressed: Department of Neurobiology, Harvard Medical School, 220 Longwood Ave., Boston, MA 02115. Phone: (617) 432-1728. Fax: (617) 734-7557. E-mail: jonathan_cohen@hms.harvard.edu.

[1] Abbreviations: ACh, acetylcholine; APFB SE, azido-2,3,5,6-tetrafluorobenzoic acid, succinimidyl ester; APFBzcholine, [2-(4-azido-2,3,5,6-tetrafluorobenzoyloxy)ethyl]trimethylammonium; nAChR, nicotinic acetylcholine receptor; Bz_2choline, 4-benzoylbenzoylcholine; Carb, carbamylcholine; PCP, phencyclidine; dTC, *d*-tubocurarine; TDBzcholine, 4-(1-azi-2,2,2-trifluoromethyl)benzoylcholine; SDS, sodium dodecyl sulfate; PAGE, polyacrylamide gel electrophoresis; HPLC, high-performance liquid chromatography; V8 protease, *S. aureus* glutamyl endopeptidase; Endo Lys-C, endoproteinase Lys-C; Endo Asp-N, endoproteinase Asp-N; α-BgTx, α-bungarotoxin; TPS, *Torpedo* physiological saline.

10.1021/bi051209y CCC: $30.25
Published on Web 09/24/2005

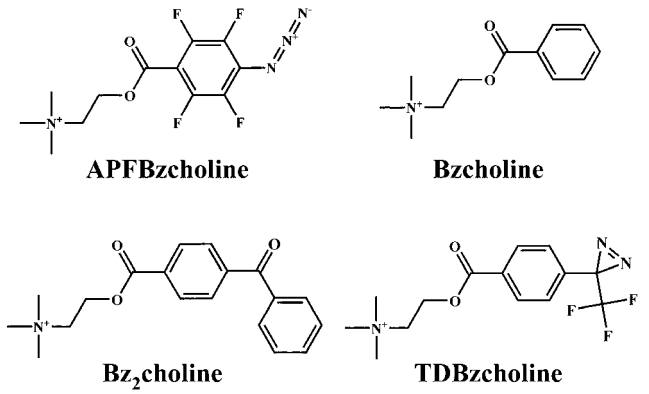

FIGURE 1: Structures of benzoylcholine derivatives.

photoreactive intermediates unknown, the studies did not define the orientation of either ligand in the transmitter binding site. [^{3}H]DCTA ([^{3}H]diazocyclohexadienylpropyltrimethylammonium), a nAChR agonist that generates on photoactivation a carbene ~6 Å from the quaternary ammonium, photolabels amino acids in the α subunit in binding site segment C (*13*). Two benzoylcholine derivatives incorporating photoreactive groups at the para position of the benzene ring have been introduced to define the orientation of aromatic choline esters in the transmitter binding site. [^{3}H]-4-Benzoylbenzoylcholine [Bz_2choline (*14*)] and [^{3}H]-4-(1-azi-2,2,2-trifluoromethyl)benzoylcholine [TDBzcholine (*15*)] are *Torpedo* nAChR competitive antagonists, which when photoincorporated at 365 nm reacted in the non-α subunits with only γLeu-109/δLeu-111. [^{3}H]TDBzcholine also reacted with αCys-192, αCys-193, and αPro-194. These results were consistent with a model in which the quaternary ammonium of these ligands occupies the core aromatic pocket of the ACh binding site with the para position of the benzoyl group oriented toward γLeu-109 (or δLeu-111) on β-strand 5 which is part of the antiparallel β sheet in the non-α subunit that forms a rigid surface at the entry to the aromatic pocket.

Although Bz_2choline and TDBzcholine acted as antagonists, benzoylcholine itself is a nAChR agonist (*16*), and we now characterize the pharmacological and photolabeling properties of [2-(4-azido-2,3,5,6-tetrafluorobenzoyloxy)ethyl]-trimethylammonium (APFBzcholine) (Figure 1). The small size of the photoreactive azide leaves APFBzcholine closer in size to benzoylcholine than those characterized previously, and we wanted to determine whether it would function as a photoreactive nAChR agonist. In addition, as a perfluoroaryl azide, formation of a highly reactive singlet nitrene is predicted to occur more favorably than for nonsubstituted aryl azides (*17*−*19*). While perfluoroaryl azides can efficiently photolabel proteins (*20*, *21*), there are few reports of the labeled amino acids. We demonstrate that APFBzcholine is a low-efficacy nAChR partial agonist which, when bound at equilibrium to the *Torpedo* nAChR, photoincorporates with UV irradiation into γLeu-109/δ-Leu-111 as well as multiple aromatic side chains within the transmitter binding sites.

EXPERIMENTAL PROCEDURES

Materials. nAChR-rich membranes (1.7 nmol of ACh sites/mg of protein) were isolated from *Torpedo californica* electric organs as described previously (*22*). 4-Azido-2,3,5,6-tetrafluorobenzoic acid, succinimidyl ester (APFBSE) was from Molecular Probes; dimethylformamide, deuterium oxide, and choline *p*-toluene sulfonate were from Sigma-Aldrich. [*methyl*-^{3}H]Choline chloride was from American Radiolabeled Chemicals (catalog no. ART-197) and [^{3}H]phencyclidine (PCP; 27 Ci/mmol) from Perkin-Elmer Life Sciences, and [^{3}H]ACh (1.9 Ci/mmol) was kindly provided by S. Hussain (Massachusetts General Hospital, Boston, MA). *Streptomyces aureus* glutamyl endopeptidase (V8 protease) and dTC were from ICN Biochemicals; endoproteinase Lys-C (Endo Lys-C) was purchased from Princeton Separations, Inc., and endoproteinase Asp-N (Endo Asp-N) was acquired from Wako Chemicals.

Synthesis of APFBzcholine. Fifty milligrams (0.15 mmol) of APFBSE was dissolved in 3 mL of anhydrous dimethylformamide and added to 130 mg (0.47 mmol) of dry choline *p*-toluene sulfonate. The reagents were coupled under argon with stirring for 24 h at 22 °C, followed by the addition of 1 mL of deionized water. The mixture was applied in four aliquots to a semipreparative reversed-phase C18 HPLC column (10 mm × 250 mm, 5 μm, 300 Å, Vydac 218TP510). Components were separated by an acetonitrile gradient of 0 to 90% over the course of 100 min at a rate of 1 mL/min, with 0.1% acetic acid present in both solvents. Absorbance was monitored at 214 and 273 nm. APFBzcholine eluted at ~40% acetonitrile; the free acid and the succinimide ester eluted at 27 and ~60% acetonitrile, respectively, and free choline eluted in the flow-through. Peak fractions were combined and dried by rotary evaporation, resuspended in methanol, and redried. The purified APFBzcholine was dissolved in 100% D_2O, and the concentration was determined by absorption at 267 nm (ϵ = 22 600 M^{-1} cm^{-1}). The reaction yield was >90% based on absorption.

The structure and purity were verified by thin-layer chromatography, NMR, and mass spectrometry. APFBzcholine was applied to a silica gel plate (Kieselgel 60 F_{254}) with the chromatogram developed in a solvent mixture made up of 1-butanol, methanol, water, and acetic acid (1:1:1:0.2, v/v/v/v). The product migrated as a single spot (R_f = 0.4) well resolved from APFB acid (R_f = 0.9), APFBSE (R_f = 1), and choline (R_f = 0.1). When the purified product, dissolved in 100% D_2O, was characterized by ^{1}H NMR (200 MHz), the following spectrum was observed: δ 7.53 (d, 1.1 H), 7.22 (d, 1.1 H), 4.71 (m, 2 H), 3.73 (t, 2 H), 3.12 (s, 9 H), 2.26 (s, 2.2 H). In addition, there was a peak at δ 1.78 (s, 0.2 H) originating from the methyl protons from the acetate salt. The ratio of protons associated with APFBzcholine to those associated with *p*-toluene sulfonate was 1.8. Electrospray ionization mass spectrometry using a Finnegan LCQ Deca instrument with an ESI probe revealed a primary mass of *m*/*z* 321.1 (exact mass of *m*/*z* 321.1 M^+) and an MS/MS fragmentation pattern consistent with the expected product.

Synthesis of [^{3}H]APFBzcholine. [^{3}H]APFBzcholine was synthesized at a radiochemical specific activity of 0.3 Ci/mmol; 1.05 mCi of [*methyl*-^{3}H]choline chloride (85 Ci/mmol, 0.011 μmol) in 1 mL of ethanol was dried under a stream of argon and resuspended in 250 μL of acetonitrile in a glass reaction vessel. To this was added 1 mg of choline *p*-toluene sulfonate (0.36 μmol) dissolved in 100 μL of acetonitrile. The isotope-diluted [^{3}H]choline chloride solution in the reaction vessel was dried under a stream of argon followed by the addition of 3.3 mg of APFB SE (1 μmol) dissolved in 27 μL of anhydrous dimethylformamide. The reaction ensued for 48 h under an argon atmosphere at 22 °C with

modest agitation; 250 μL of an 80:20 water/acetonitrile mixture was added to the reaction mixture, and the crude mixture was applied in three aliquots to an analytical reversed-phase HPLC column (3.9 mm × 300 mm, 10 μm, C18, Waters μBondapak catalog no. 27324). Components were separated by a gradient of acetonitrile from 0 to 90% over the course of 54 min at a rate of 0.75 mL/min with 0.04% acetic acid present in both solvents. Elution of ^{3}H was assessed by scintillation counting. Peak fractions were pooled, concentrated by rotary evaporation, resuspended in 600 μL of argon-purged ethanol, and stored at −80 °C. Purity was analyzed by thin-layer chromatography in which 1 μL of a 1:100 dilution of the purified radioactive product was coapplied with nonradioactive APFBzcholine to a silica gel plate and the chromatogram developed as described above. The developed plate was then exposed to a tritium sensitive phosphor screen (Kodak model 890 8972) for 16 h followed by imaging using a Storm Phosphorimager (Molecular Dynamics). A single peak of radioactivity was present that comigrated with nonradioactive APFBzcholine (R_f = 0.4). The final yield was 0.75 mCi.

Electrophysiology. The agonist and/or antagonist actions of APFBzcholine and benzoylcholine on wild-type *Torpedo* and mouse $\alpha_2\beta\gamma\delta$ nAChRs expressed in *Xenopus* oocytes were measured by standard two-electrode voltage clamp (Oocyte clamp OC-725B, Warner Instrument) techniques as described previously (*15*). Solutions of drugs were made in low-calcium ND96 recording solution [96 mM NaCl, 2 mM KCl, 0.3 mM $CaCl_2$, 1 mM $MgCl_2$, and 5 mM HEPES (pH 7.6)] containing 1 μM atropine.

Radioligand Binding Assays. The equilibrium binding of [^{3}H]ACh or [^{3}H]PCP to *Torpedo* nAChR-rich membranes in *Torpedo* physiological saline (TPS) [250 mM NaCl, 5 mM KCl, 3 mM $CaCl_2$, 2 mM $MgCl_2$, and 5 mM $NaPO_4$ (pH 7.0)] was assessed by centrifugation as described previously (*23*). Membrane suspensions were pretreated with diisopropyl phosphofluoridate (~0.5 mM) for 20 min to inhibit acetylcholinesterase activity. Dilute membrane suspensions (1 mL, 84 μg of protein/mL, 40 nM ACh binding sites) were used for the [^{3}H]ACh (70 nM) binding assay, whereas the binding of [^{3}H]PCP (6 nM) was assessed at 700 μg of protein/mL, in a volume of 200 μL, and in the absence or presence of 1 mM Carb or 4 μM α-bungarotoxin (α-BgTx). The equilibrium binding of [^{3}H]APFBzcholine was assessed at 2 mg of protein/mL (100 μL, 3 μM [^{3}H]ACh binding sites). Membrane suspensions were equilibrated with [^{3}H]ACh and [^{3}H]APFBzcholine for 45 min and with [^{3}H]PCP for 2 h prior to centrifugation. Nonspecific binding of [^{3}H]ACh or [^{3}H]APFBzcholine was assessed in the presence of 1 mM Carb, while that of [^{3}H]PCP was assessed in the presence of 1 mM proadifen (with Carb) or 1 mM tetracaine (without Carb).

Data Analysis. For nAChR activation, dose−response curves were fit to eq 1:

$$I/I_{max} = [1 + (K_{app}/x)^n]^{-1} \quad (1)$$

where I and I_{max} are the current at agonist concentration x and the maximum current, respectively, K_{app} is the agonist concentration producing a half-maximal response, and n is the Hill coefficient. The concentration dependence of APFBzcholine inhibition of ACh-induced currents or radioligand binding was fit to eq 2:

$$f(x) = f_0/[1 + (x/IC_{50})^n] + f_{ns} \quad (2)$$

where $f(x)$ is the current or total ^{3}H-labeled radioligand bound in the presence of inhibitor concentration x, f_0 is the current or specific radioligand bound in the absence of inhibitor, f_{ns} is the leak current in the absence of ACh or nonspecific radioligand binding, IC_{50} is the inhibitor concentration associated with 50% inhibition of ACh-induced currents or radioligand binding, and n is the Hill coefficient. The concentration-dependent inhibition of [^{3}H]ACh binding by dTC was fit to a two-site model as shown in eq 3:

$$f(x) = (0.5f_0)/(1 + x/K_H) + (0.5f_0)/(1 + x/K_L) \quad (3)$$

where $f(x)$ is the level of total [^{3}H]ACh binding measured in the presence of dTC concentration x, f_0 is the level of [^{3}H]ACh binding measured in the absence of dTC, and K_H and K_L are the dissociation constants for the high- and low-affinity binding sites, respectively. Equilibrium binding data for [^{3}H]APFBzcholine were fit to a single-site model with a linear nonspecific binding component as shown in eq 4:

$$B(x) = B_{max}/(1 + K_{eq}/x) + mx \quad (4)$$

where $B(x)$ is the [^{3}H]APFBzcholine bound at a free concentration x, B_{max} is the concentration of [^{3}H]APFBzcholine binding sites, K_{eq} is the dissociation constant, and m is the slope of nonspecific binding derived from parallel experiments performed in the presence of 1 mM Carb. SigmaPlot (SPSS) was used for the nonlinear least-squares fit of the data, and the standard errors of the parameter fits are indicated.

Photolabeling nAChR-Rich Membranes with [^{3}H]APFBzcholine. Freshly thawed nAChR-rich *Torpedo* membranes were pretreated with diisopropyl phosphofluoridate (~0.5 mM) for 20 min to inhibit acetylcholinesterase activity, diluted ≥3-fold with TPS, and pelleted. The pellets were resuspended at 2 mg of protein/mL (~3 μM ACh binding sites) in TPS with 1 mM oxidized glutathione added as noted to serve as an aqueous scavenger. [^{3}H]APFBzcholine (0.3 Ci/mmol) was added to the membrane suspension and agitated for 20 min prior to the addition of other drugs. For photolabeling on an analytical scale, samples were equilibrated with [^{3}H]APFBzcholine (33 μM) and additional cholinergic ligands for 90 min at 4 °C in polypropylene microfuge tubes shielded from light, and then 120 μL (240 μg of protein) aliquots were placed in a 96-well polystyrene microtiter plate (Costar model 9017). The wavelength dependence of photolabeling was tested by irradiating samples with 254 (Spectroline EF-16), 312 (Spectroline EB-280C), or 365 nm light (Spectroline EN-16) at a distance of 6 cm. For preparative photolabeling, membrane suspensions (10 mg of protein per condition, 2 mg/mL in TPS and 1 mM oxidized glutathione) were equilibrated with [^{3}H]APFBzcholine (40 μM) and 100 μM proadifen (a desensitizing aromatic amine noncompetitive antagonist) (*24*) in the presence or absence of 1 mM Carb and incubated for 30 min at 4 °C, and then 5 mL aliquots were placed in 2.5 cm plastic Petri dishes. The suspensions, on ice, were irradiated at 254 nm for 6 min.

SDS−PAGE. Photolabeled membranes were solubilized in sample buffer and separated on 1.5 mm, 8% acrylamide gels (*25*). Analytical gels were stained with Coomassie Blue and preparative gels with GelCode Blue Stain Reagent (Pierce). After staining, the analytical gels were prepared for fluorography and/or bands of interest were excised for determination of the extent of ^{3}H incorporation by liquid scintillation counting. After photolabeling at the preparative scale, the δ subunit was isolated by passive elution of the excised gel bands and the α and γ subunit bands were excised and placed in the wells of 15 cm long, 15% acrylamide gels for controlled "in-gel" digestion with V8 protease (1:10 protease:subunit protein ratio) (*25*). Because preliminary experiments indicated that [^{3}H]APFBzcholine photoincorporation was potentially unstable under prolonged isolation procedures, material from the V8 mapping gels was directly electroeluted from the intact gels in 5 mm bands with a Bio-Rad Whole Gel Electroeluter. The elution buffer contained 50 mM Tris, 25 mM boric acid (pH 8.7), and 0.1% SDS. The α and γ subunit V8 mapping gels were eluted at 250 mA for 30 min and at 200 mA for 25 min, respectively. Fractions of ∼3 mL were collected from each band, and ∼1% was assayed for ^{3}H. Fractions of interest were filtered and concentrated by vacuum centrifugation to <500 μL, acetone precipitated in 75% acetone (−20 °C, >2 h), and then resuspended in a buffer appropriate for enzymatic digestion.

Reversed-Phase HPLC. Digests and gel-purified samples were fractionated by reversed-phase HPLC on an Agilent 1100 system with a column heater, a solvent degasser, and an external absorbance detector (Kratos Spectroflow 757) set at 214 nm. Separations were achieved at 40 °C using a 10 cm Brownlee Aquapore Butyl 7 micron column with an upstream C-2 guard column. Solvent A was 0.04% trifluoroacetic acid, while solvent B consisted of 60% acetonitrile, 40% 2-propanol, and 0.025% trifluoroacetic acid. The gradients that were used are included on the chromatograms in Figures 7 and 8 as dashed lines. The flow rate was 200 μL/min with fractions collected every 2.5 min into 1.5 mL tubes containing 30 μL of 100 mM phosphate buffer (pH 7.8) to limit the acid exposure of the labeled material (final pH of test fractions was ∼5.5).

Enzymatic Digestions. For digestion with Endo Lys-C (0.5 μg, 32 °C, 36 h), material was resuspended in 25 mM Tris buffer (pH 8.6) containing 0.1% SDS and 0.5 mM EDTA. The same buffer was used to resuspend samples for digestion with Endo Asp-N, but the samples were subsequently diluted to 5 mM Tris (pH 8.6), 0.02% SDS, and 0.1 mM EDTA with water prior to the addition of the enzyme (0.2 μg, 32 °C, 36 h).

Amino Acid Sequence Analysis. N-Terminal sequence analysis was performed on an Applied Biosystems Procise 492 protein sequencer. HPLC fractions of interest were drop loaded onto Biobrene-treated glass fiber filters (AB #601111). Samples containing detergent and many HPLC samples were washed on the sequencer with a pretreatment of gas trifluoroacetic acid (4 min) followed by consecutive washes with *N*-butyl chloride and ethyl acetate (5 min each) to remove excess detergent and/or buffer salts. Twenty microliters ($^1/_6$) of each cycle was analyzed for residue detection and quantitation, whereas 100 μL was collected for scintillation counting. Amino acid amounts were determined by peak heights, and the amount of each peptide was obtained from a nonlinear least-squares fit (Sigma Plot) of the equation $f(x) = I_0R^x$, where $f(x)$ is the number of picomoles of the peptide's residue in cycle x, I_0 is the initial amount of peptide (in picomoles), and R is the average repetitive yield of the sequencer. Ser, Cys, Arg, His, and Trp residues were excluded from the fit due to known problems with their quantitations. Plots of these fits are included in the sequence graphs as dotted lines. Unless otherwise noted, the efficiency of labeling of amino acid residues [counts per minute (cpm) per picomole] was calculated by the equation $(\mathrm{cpm}_x - \mathrm{cpm}_{x-1})/(5I_0R^x)$.

Molecular Modeling. A model of the extracellular region of the *Torpedo* nAChR, constructed from the structure of the snail acetylcholine binding protein [PDB entry 1I9B (*26*)] using the homology module of Insight II (*27*), was used at a pH 7.0 protonation state. Docking of APFBzcholine was performed using the Docking module of Insight II (Accelrys). Because the cvff force field used for the Docking module does not accept an azide, it was replaced by a C═C═O. For docking, only the α and γ subunit pair was used. The binding site was defined as all amino acids within 6 Å of the APFBzcholine homologue which was initially placed within the agonist binding site with the quaternary nitrogen inside the core aromatic binding pocket. Although the program sampled >14000 orientations using three translational degrees of freedom (maximum of 3 Å) and three rotational degrees of freedom (maximum of 180°), only one orientation was obtained (>60 times, Figure 8). The energies of interaction for this orientation were −59 kcal/mol for the van der Waals force calculation and −476 kcal/mol for the electrostatic calculation, and the carbonyl oxygen of the APFBzcholine was oriented to form a hydrogen bond with the hydroxyl of αTyr-198. In this orientation, the distances (angstroms) from the nitrogen forming the nitrene after photoactivation to the binding site amino acids in γ were as follows: γTyr-117, 3.9; γGln-59, 4.1; γGlu-57, 5.7; γLeu-109, 6.4; γLeu-119, 7.5; γLeu-77, 7.8; γTyr-111, 8.4; and γTrp-55, 11.1. For the α subunit the distances were as follows: αPro-194, 4.8; αCys-193, 6.2; αCys-192, 7.5; αTyr-198, 7.5; and αTyr-190, 11.2.

RESULTS

APFBzcholine and Benzoylcholine as nAChR Agonists. We used two-electrode voltage clamp to compare the interactions of APFBzcholine and benzoylcholine with wild-type *Torpedo* and embryonic mouse nAChR expressed in *Xenopus* oocytes. Both nAChRs were examined because ACh gates the mouse nAChR with higher efficacy than the *Torpedo*, and we wanted to determine whether APFBzcholine was a low-efficacy agonist. APFBzcholine activated the mouse nAChR (Figure 2), producing a maximal response that was 0.3 ± 0.1% of that of ACh with a K_{app} of 170 ± 80 μM (n = 5). In comparison, for benzoylcholine the maximal response was 1.4 ± 0.4% of that of ACh with a K_{app} of 350 ± 20 μM (n = 5). For the *Torpedo* nAChR, benzoylcholine was a partial agonist producing a maximal response that was 0.2 ± 0.1% of that of ACh with a K_{app} of 80 μM, and 1 mM APFBzcholine produced a maximal response (∼40 nA) that was ∼0.1% of that of ACh (n = 2; values of K_{app} were not determined because of the small currents). When coapplied with 10 μM ACh, APFBzcholine produced a fully reversible,

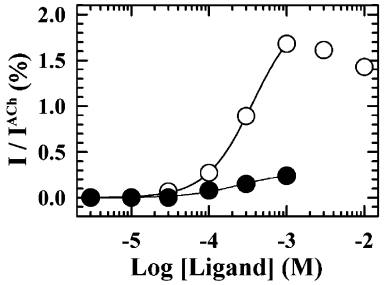

FIGURE 2: APFBzcholine and benzoylcholine are embryonic mouse nAChR partial agonists. Currents (I) elicited by APFBzcholine (●) or benzoylcholine (○) for mouse nAChRs expressed in *Xenopus* oocytes were measured by a two-electrode voltage clamp and normalized to the maximal current evoked by ACh (I^{ACh}). Three current measurements were taken at each test concentration, with means plotted (and the standard error of the mean smaller than the symbol sizes).

concentration-dependent inhibition of ACh currents characterized by an IC_{50} of 16 μM and a Hill coefficient of 1 (Figure 3A), whereas for benzoylcholine, the IC_{50} was 40 μM (not shown).

Since these results revealed that the agonist responses of low-efficacy partial agonists such as benzoylcholine and APFBzcholine were more readily detected for mouse than for *Torpedo* nAChRs, we also examined whether Bz_2choline or TDBzcholine activated mouse nAChR. Although no detectable responses had been seen by two-electrode voltage clamp for *Torpedo* nAChRs in oocytes [with an upper limit of currents that was <0.1% of that of ACh (*14*, *15*)], both ligands activated the mouse nAChR with maximal responses that were 0.1% of that of ACh and a K_{app} of 30 ± 10 μM (Bz_2choline, $n = 2$) or 70 μM (TDBzcholine, $n = 1$).

Effects of APFBzcholine on the Equilibrium Binding of [^{3}H]ACh and [^{3}H]Phencyclidine. In equilibrium binding studies with *Torpedo* nAChR-rich membranes, APFBzcholine fully inhibited the specific binding of [^{3}H]ACh (70 nM), with a concentration dependence of inhibition being fit well by a single-site model with an IC_{50} of 27 μM (Figure 3B). We also assessed under identical conditions the inhibition of [^{3}H]ACh binding by the competitive antagonist *d*-tubocurarine (Figure 3B) and found, as expected (*28*), that the data were fit well by a two-site model with a K_H of 120 nM and a K_L of 37 μM. The noncompetitive antagonist [^{3}H]phencyclidine (PCP) binds with high affinity ($K_{eq} = 1$ μM) to a single site per receptor in the desensitized state (in the presence of agonist) and more weakly ($K_{eq} = 7$ μM) in the absence of agonist (*29*). In the absence of APFBzcholine, the level of total binding of [^{3}H]PCP to *Torpedo* membranes was 4-fold greater in the presence of agonist (Carb) than in its absence or in the presence of α-bungarotoxin (α-BgTx, a competitive antagonist that stabilizes the closed state of the receptor). APFBzcholine inhibited the binding of [^{3}H]PCP with IC_{50} values of 850 and 1700 μM in the presence of Carb and α-BgTx, respectively (Figure 3C). In the absence of agonist, at concentrations between 1 and 100 μM, APFBzcholine increased the level of [^{3}H]PCP binding by 200%, with inhibition occurring at concentrations above 100 μM. These results establish that APFBzcholine binds with similar affinities to both ACh binding sites in the *Torpedo* nAChR and also with 30−60-fold lower affinity to an additional site, probably within the ion channel.

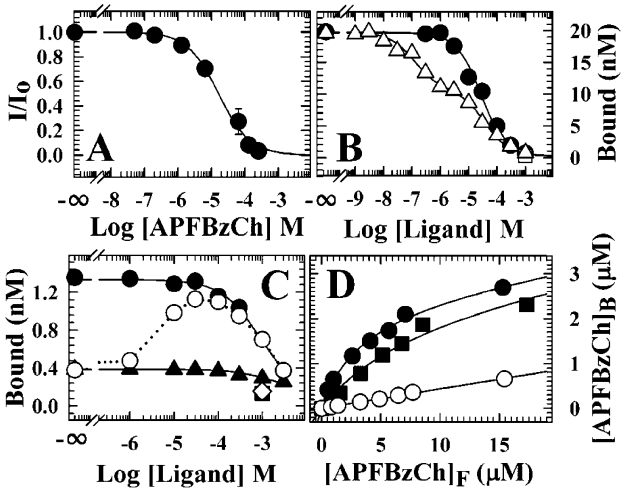

FIGURE 3: Interactions of APFBzcholine with *Torpedo* nAChRs. (A) APFBzcholine inhibition of ACh current responses for *Torpedo* nAChRs expressed in *Xenopus* oocytes. Currents (I) elicited by 10 μM ACh in the presence of APFBzcholine were measured by a two-electrode voltage clamp and normalized to the current (I_0) in the absence of APFBzcholine. The IC_{50} was 16 ± 1 μM with a Hill coefficient of 1.1 ± 0.1. (B) APFBzcholine (●) and *d*-tubocurarine (△) inhibition of the equilibrium binding of [^{3}H]ACh (70 nM) to *Torpedo* nAChR-rich membranes. The inhibition of [^{3}H]ACh binding was characterized by an IC_{50} of 27 ± 4 μM for APFBzcholine (eq 1; n fixed at l) and by a K_H of 0.12 ± 0.03 μM and a K_L of 37 ± 7 μM for dTC (eq 3; two-site model). (C) Effects of APFBzcholine on the equilibrium binding of [^{3}H]PCP (6 nM) to *Torpedo* nAChR-rich membranes in the absence (○) or presence of 1 mM Carb (●) or 4 μM α-BgTx (▲). In the absence of Carb or α-BgTx, APFBzcholine potentiated binding with an EC_{50} of 5 μM and then inhibited binding at concentrations above 100 μM. The inhibition of [^{3}H]PCP binding in the presence of Carb or α-BgTx was characterized by an IC_{50} value of 850 ± 70 μM or 1.7 ± 0.3 mM, respectively. Proadifen (1 mM, ■) was used to define nonspecific binding in the presence of Carb, and tetracaine (1 mM, ◇) was used in its absence. (D) Equilibrium binding of [^{3}H]-APFBzcholine to nAChR-rich membranes was assessed by centrifugation in the absence (■) or presence (●) of 100 μM proadifen or in the presence of 1 mM Carb and 100 μM proadifen (○). The calculated K_{eq} values were 12 ± 2 and 4.1 ± 0.5 μM in the absence and presence of proadifen, respectively. The concentrations of APFBzcholine binding sites were calculated to be 1.7 nmol/mg of protein without proadifen and 1.5 nmol/mg of protein with proadifen, whereas that of ACh binding sites was 1.5 nmol/mg of protein.

Equilibrium Binding of [^{3}H]APFBzcholine. The equilibrium binding of [^{3}H]APFBzcholine to nAChR-rich membranes was assessed in the absence or presence of proadifen, a desensitizing noncompetitive antagonist (Figure 3D). The level of [^{3}H]APFBzcholine binding in the presence of both proadifen and Carb, which increased linearly with the free concentration, was used as a measure of the the level of nonspecific binding. The level of specific binding of [^{3}H]APFBzcholine was fit well by a simple hyperbolic binding function characterized by K_{eq} values of 12 and 4 μM in the absence and presence of proadifen, respectively. The concentration of [^{3}H]APFBzcholine binding sites [1.7 nmol/mg (without proadifen) or 1.5 nmol/mg (with proadifen)] was close to the concentration of [^{3}H]ACh sites (1.5 nmol/mg).

Photoincorporation of [^{3}H]APFBzcholine into nAChR-Rich Membranes. We first compared the pattern of [^{3}H]APFBzcholine photoincorporation into nAChR-rich membranes resulting from UV irradiation at 254, 312, and 365

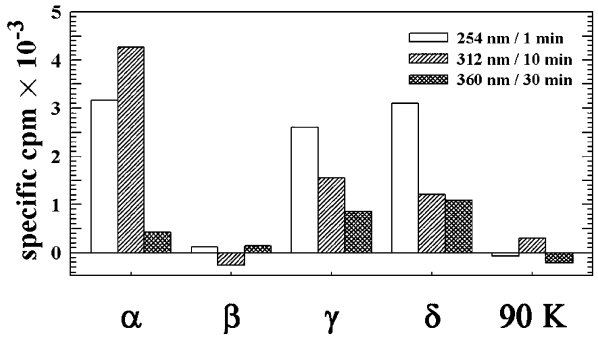

FIGURE 4: Wavelength dependence of [^{3}H]APFBBzcholine photolabeling of *Torpedo* nAChR-rich membranes. nAChR-rich membranes (200 μg, 200 pmol of ACh sites in 100 μL of TPS) were equilibrated with 30 μM [^{3}H]APFBzcholine in the absence or presence of 1 mM Carb. Samples were irradiated at 254 (1 min), 312 (10 min), or 360 nm (30 min), and then polypeptides were resolved by SDS−PAGE and visualized by Coomassie Blue stain. The nAChR subunits and the Na^+/K^+-ATPase α subunit (90K) were excised from the gel, and the extent of ^{3}H incorporation was determined by liquid scintillation counting. The level of specific incorporation was calculated for each band as the difference between the level of ^{3}H incorporation for the sample without Carb and with Carb. Depending upon the band, the values (with Carb) were 800−1200 cpm for 254 nm, 1500−1900 cpm for 312 nm, and 500−700 cpm for 365 nm.

nm. After SDS−PAGE, covalent incorporation into the nAChR subunits or other polypeptides was assessed by liquid scintillation counting of excised gel bands. For irradiation at 365 nm, agonist-inhibitable labeling was restricted to the nAChR γ and δ subunits, while for irradiation at 254 or 312 nm, there was also agonist-inhibitable labeling in the α subunit (Figure 4). The effectiveness of oxidized glutathione (1 mM) as an aqueous scavenger was tested for 254 nm irradiation. It reduced the level of nonspecific subunit labeling seen in the presence of agonist by 30%, while reducing the level of specific (agonist-inhibitable) labeling in the α subunit by 15% and in γ and δ subunits by <5%. On the basis of these results, further photolabeling studies were carried out with 254 nm irradiation in the presence of oxidized glutathione.

The pharmacological specificity of the nAChR photolabeling at the subunit level was further characterized by photolabeling membranes at 254 nm with [^{3}H]APFBzcholine (33 μM) in the absence of other drugs and in the presence of an agonist (Carb), a competitive antagonist (α-BgTx), a desensitizing noncompetitive antagonist (proadifen), or a nondesensitizing noncompetitive antagonist (tetracaine), with the labeling pattern characterized by fluorography (Figure 5A) and by liquid scintillation counting of excised gel bands (Figure 5B). Carb (lane 3, Figure 5A) or α-BgTx (lane 4) inhibited photolabeling in the nAChR α subunit by ∼80% and in the γ and δ subunits by ∼60%. In the presence of proadifen (lane 5), the extent of labeling in the γ and δ subunits was increased by ∼75−100%, while tetracaine (lane 6) caused a <10% change. The subunit labeling in the presence of Carb and proadifen (lane 7) was similar to that seen in the presence of Carb alone. On the basis of the radiochemical specific activity of [^{3}H]APFBzcholine, the agonist-inhibitable ^{3}H incorporation indicated specific labeling of the α, γ, and δ subunits at 5−6% each, with any specific labeling of the β subunit at <0.5%. On the basis of the lack of proadifen-inhibitable subunit labeling in the

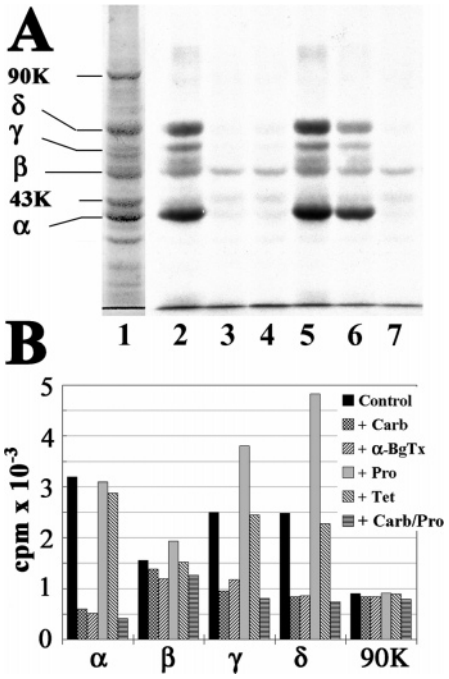

FIGURE 5: Effects of nAChR agonists and antagonists on the photoincorporation of [^{3}H]APFBBzcholine into nAChR-rich membranes. nAChR-rich membranes (240 μg, 250 pmol of ACh sites in 120 μL of TPS supplemented with 1 mM oxidized glutathione) were equilibrated with 33 μM [^{3}H]APFBzcholine either alone (control, lane 2) or with 1 mM Carb (lane 3), 6 μM α-BgTx (lane 4), 100 μM proadifen (lane 5), 100 μM tetracaine (lane 6), or 1 mM Carb and 100 μM proadifen (lane 7). Samples were irradiated at 254 nm for 5 min. (A) Polypeptides were resolved by SDS−PAGE, visualized by Coomassie Blue stain (lane 1), and processed for fluorography (lanes 2−8, 30-day exposure). Indicated on the left are the stained bands corresponding to the nAChR subunits, rapsyn (43K), and the α subunit of the Na^+/K^+-ATPase (90K). (B) After fluorography, the visualized subunit bands were excised, and the level of ^{3}H incorporation was determined by liquid scintillation counting.

presence of Carb or tetracaine-inhibitable labeling in the presence of αBgTx, there was no evidence of substantial channel photolabeling for nAChRs in either the closed or desensitized state. In contrast, [^{3}H]Bz$_2$choline and [^{3}H]TDBzcholine photoincorporated into the ion channel in the closed state (*14*, *15*).

Identification of the Amino Acids Photolabeled by [^{3}H]APFBzcholine in the γ Subunit. To identify the sites of [^{3}H]APFBzcholine photoincorporation within the γ subunit, nAChR-rich membranes (10 mg aliquots) equilibrated with [^{3}H]APFBzcholine (40 μM) and 100 μM proadifen and in the absence or presence of 1 mM Carb were irradiated at 254 nm for 6 min, and then polypeptides were separated by SDS−PAGE on an 8% acrylamide gel. The bands containing the nAChR γ subunit were excised from the stained gels and placed in the well of a second 15% acrylamide gel for in-gel digestion with V8 protease (see Experimental Procedures). After electrophoresis and electroelution (5 mm of gel/fraction), ∼45% of recovered ^{3}H in samples labeled in the absence of Carb was in fractions 21 and 22 corresponding to a gel band of ∼14 kDa, while the amount of ^{3}H in corresponding fractions from samples labeled in the presence of Carb was reduced by ∼90% (Figure 6A). When gel eluate fractions 21 and 22 were pooled and the material was further purified by reversed-phase HPLC (Figure 6B), ∼55% of the

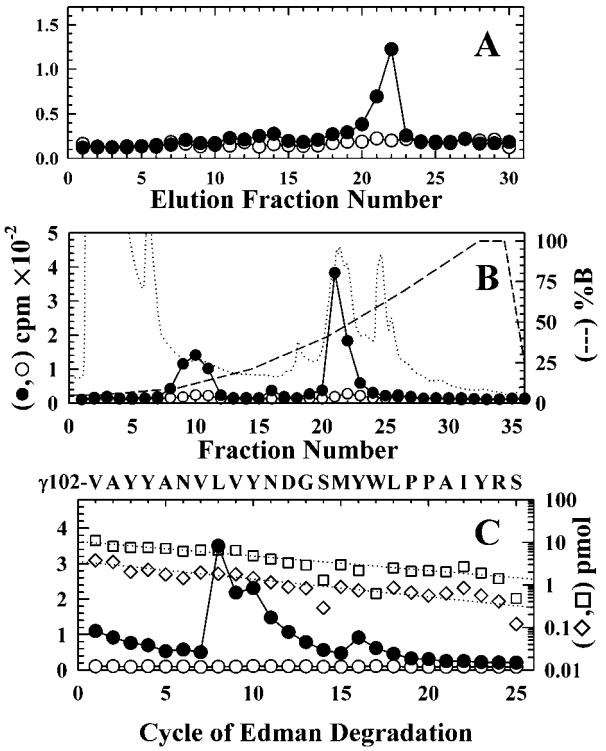

FIGURE 6: Identification of nAChR γ subunit amino acids photolabeled with [^{3}H]APFBzcholine. nAChR-rich membranes (10 mg of protein in 5 mL of TPS with 1 mM oxidized glutathione and 3.4 μM ACh sites) were photolabeled with [^{3}H]APFBzcholine (40 μM) in the presence of 0.1 mM proadifen and in the absence (●) or presence (○) of 1 mM Carb (10 mg of protein each), and the γ subunit bands were excised from a Coomassie-stained 8% gel and placed on additional slab gels for in-gel digestion with V8 protease (see Experimental Procedures). (A) ^{3}H elution profile of material eluted directly from the mapping gel (~1% of each fraction counted; fraction 1 is the top and 30 the bottom of the resolving gel). (B) ^{3}H elution profile when gel fractions 21 and 22 were further purified by reversed-phase HPLC, with 10% of each fraction assayed for ^{3}H (●, without Carb, 13 400 cpm injected, 11 200 cpm recovered; ○, with Carb, 1060 cpm injected, 1100 cpm recovered). Also plotted are the absorption at 214 nm (···) and the percent solvent B (− − −). (C) ^{3}H (● and ○) and mass release (□ and ◇) when HPLC fraction 21 was sequenced for 25 cycles (●, without Carb, 3340 cpm loaded, 335 cpm remaining on the filter; ○, with Carb, 90 cpm loaded, 10 cpm remaining). The primary sequence began at γVal-102 (□, without Carb, $I_0 = 10.4 \pm 0.6$ pmol, $R =$ 93%; ◇, with Carb, $I_0 = 3.6 \pm 0.2$ pmol, $R = 92\%$) and secondary sequences at γAla-49 (without Carb, $I_0 = 0.6$ pmol) and V8 protease Val-1 ($I_0 = 3$ pmol). The ^{3}H releases in cycles 8 (300 cpm), 10 (80 cpm), and 16 (44 cpm) of the sample without Carb are consistent with the labeling of γLeu-109 (11 cpm/pmol), γTyr-111 (3 cpm/pmol), and γTyr-117 (3 cpm/pmol). The extent of ^{3}H release of 80 cpm was calculated for cycle 10 with an assumption of exponential decay of the release from cycle 8 to determine the background at cycle 10. Sequence analysis of HPLC fractions 9−11 (in panel B) revealed no detectable amino acids.

^{3}H was recovered in a hydrophobic peak (fractions 21 and 22, ~45% solvent B), and ~30% in a hydrophilic peak (fractions 9−11, which upon sequence analysis contained no released ^{3}H or PTH-amino acids).

Sequence analysis of fraction 21 (Figure 6C) revealed a primary sequence beginning at γVal-102 ($I_0 = 10$ pmol), a secondary sequence beginning at γAla-49 ($I_0 = 0.6$ pmol), and a fragment beginning at V8 protease Val-1 ($I_0 = 3.3$ pmol). For the sample without Carb there was ^{3}H release in cycles 8 (300 cpm), 10 (80 cpm), and 16 (44 cpm), consistent with [^{3}H]APFBzcholine incorporation at γLeu-109 (11 cpm/pmol), γTyr-111 (3 cpm/pmol), and γTyr-117 (3 cpm/pmol) from the γVal-102 peptide. Sequence analysis of fraction 22 (without Carb, not shown) revealed the presence of the same three peptides, but at different relative amounts (2.8 pmol of γVal-102, 1.2 pmol of γAla-49, and 1.2 pmol of V8 protease Val-1). For that sample, there was ^{3}H release in cycles 8 (67 cpm), 10 (23 cpm), and 16 (18 cpm), consistent with incorporation at γLeu-109 (8 cpm/pmol), γTyr-111 (3 cpm/pmol), and γTyr-117 (4 cpm/pmol). There was no ^{3}H release in cycle 7 (<3 cpm), which for the γAla-49 fragment is the cycle containing γTrp-55, the core aromatic of agonist binding site segment D that is photolabeled by [^{3}H]dTC and [^{3}H]nicotine (*11*, *12*). On the basis of the amount of γAla-49 fragment, if there is labeling of γTrp-55, it is at a level of <0.7 cpm/pmol.

Identification of the Amino Acids Photolabeled by [^{3}H]APFBzcholine in the δ Subunit. To determine whether the amino acids photolabeled in the δ subunit included δLeu-111, which is homologous to γLeu-109, or nearby amino acids, the isolated δ subunits were digested with Endo Asp-N, which generates a fragment beginning at δAsp-99 (*14*). When the digests were fractionated by reversed-phase HPLC (Figure 7A), there was a complex ^{3}H elution profile with a major ^{3}H peak in fraction 22 (44% solvent B) and additional peaks or shoulders at fractions 18, 24, and 27 and the flow-through (fraction 3). Sequence analysis (Figure 7B) of an aliquot of fraction 22 (without Carb) revealed the presence of four peptides beginning at δAsp-99 ($I_0 = 8$ pmol), δAsp-76 ($I_0 = 15$ pmol), δAsp-10 ($I_0 = 4$ pmol), and δAsp-171 ($I_0 = 4$ pmol), with ^{3}H release in cycle 13 (111 cpm), consistent [^{3}H]APFBzcholine incorporation at δLeu-111 (7 cpm/pmol), and additional release in cycle 4 (48 cpm).

The HPLC fractions surrounding fraction 22 were also sequenced to confirm that the ^{3}H release in cycle 13 was associated with the δAsp-99 peptide and to determine which fragment was the source of ^{3}H release in cycle 4 (Figure 7C−H). The ^{3}H releases in cycles 13 and 4 were largest for fraction 22, and their magnitudes correlated well with the number picomoles in each fraction of the fragments beginning at either δAsp-99 or δAsp-76, but not with those beginning at δAsp-10 or δAsp-171 (which contains amino acids of agonist binding site segment F). Since δTyr-103, which would be labeled if the ^{3}H release in cycle 4 originated from the δAsp-99 fragment, is known to be in the vestibule of the channel and not near the agonist binding site (*30*), the ^{3}H release in cycle 4 may result from labeling of δIle-79 of the δAsp-76 fragment, which is positioned on β strand 3 and adjacent to δLeu-111 (see Figure 8). However, further studies are necessary to confirm this.

Sequence analysis of HPLC fractions 27 and 28 revealed the presence of multiple peptides, including δAsp-99 (1.5 pmol), with ^{3}H release in cycle 13 (35 cpm) consistent with labeling of δLeu-111 at a level of 11 cpm/pmol. There was no ^{3}H release above background when HPLC fraction 3 was sequenced, which contained multiple small peptides fewer than eight amino acids in length.

[^{3}H]APFBzcholine Photoincorporation in the α Subunit. To determine the regions of the α subunit containing the agonist-inhibitable photolabeling, the labeled α subunits were digested in gel with V8 protease which generates four nonoverlapping subunit fragments, including a 20 kDa fragment (αV8−20) that begins at αSer-173 and contains

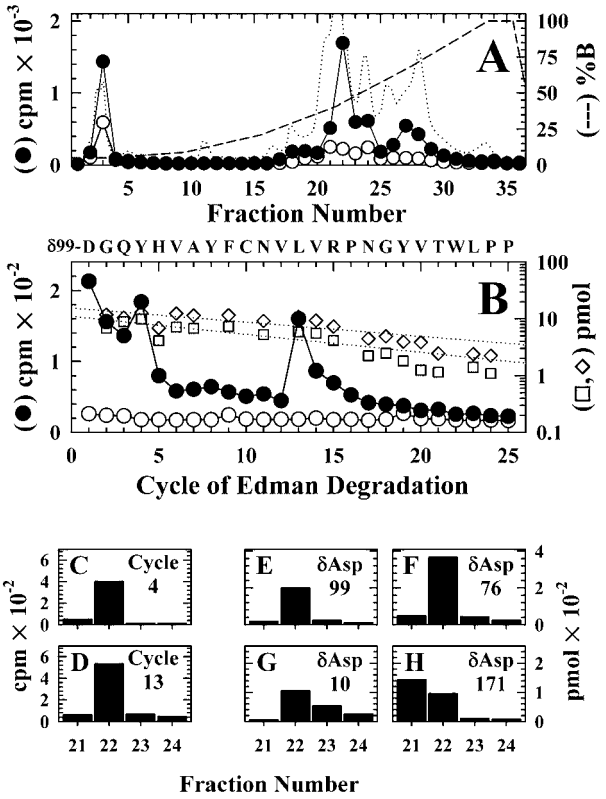

FIGURE 7: [^{3}H]APFBzcholine photolabels δLeu-111. Labeled δ subunits isolated from the photolabeling described in the legend of Figure 5 of nAChR-rich membranes in the absence (●, without Carb) or presence (○, with Carb) of agonist were digested with Endo Asp-N. (A) The digests were fractionated by reversed-phase HPLC (without Carb, 87 800 cpm injected, 78 400 cpm recovered; with Carb, 34 000 cpm injected, 25 460 cpm recovered) with 10% of each fraction assayed for ^{3}H and the absorption monitored at 214 nm (⋯). (B) ^{3}H (● and ○) and mass release (□ and ◇) when an aliquot of fraction 22 was sequenced for 25 cycles (●, without Carb, 4040 cpm loaded, 30 cpm collected in the prewash, 275 cpm remaining on the filter; ○, with Carb, 515 cpm loaded, 135 cpm remaining). δ subunit fragments were identified beginning at δAsp-99 (□, without Carb, $I_0 = 8 \pm 1$ pmol, $R = 93\%$; ◇, with Carb, $I_0 = 16 \pm 1$ pmol, $R = 94\%$), δAsp-76 (without Carb, $I_0 = 15$ pmol, $R = 91\%$), δAsp-10 (without Carb, $I_0 = 4$ pmol, $R = 90\%$), and δAsp-171 (~4 pmol). Release of ^{3}H was detected in cycle 13 (110 cpm), consistent with incorporation at δLeu-111 (6.5 cpm/pmol), and also in cycle 4 (48 cpm). Sequence analysis of the HPLC flow-through (fraction 3 in panel A) revealed numerous small peptides with no ^{3}H release in 20 cycles. (C−H) Comparison of the ^{3}H release in cycles 4 (C) and 13 (D) with the amounts of δAsp-99 (E), δAsp-76 (F), δAsp-10 (G), and δAsp-171 (H) peptides present in HPLC fractions 21−24. Both the counts per minute released and the picomoles of each peptide are the amounts calculated for the entire HPLC fraction. Fraction 21 also contained peptides beginning at δGlu-380 (190 pmol) and δAsp-354 (96 pmol).

the amino acids in agonist binding site segment C and the M1−M3 membrane-spanning segments and an 18 kDa fragment (αV8−18) that begins at αThr-52 and contains binding site segments A and B (*25*). We found that ~90% of the Carb-inhibitable [^{3}H]APFBzcholine incorporation was in the αV8−20 fragment and that <10% was in αV8−18 (data not shown). To determine whether there was incorporation of ^{3}H in amino acids within binding site segment C, αV8−20 was isolated from nAChRs labeled on a preparative scale by direct electroelution from the V8 mapping gel and then digested with Endo Lys-C, which cleaves after αLys-179 and αLys-185 (*15*). When aliquots of the digests were sequenced (without Carb, 1300 cpm; with Carb, 400 cpm), multiple peptides from αV8−20 were identified, including the one beginning at αHis-186 ($I_0 = 2$ pmol), and there was ^{3}H release in cycle 13 (34 cpm), which would correspond to labeling of αTyr-198 at 20 cpm/pmol, as well as lower-level release in cycles 5 (12 cpm), 7 (7 cpm), and 8 (8 cpm), corresponding to αTyr-190, αCys-192, and αCys-193, respectively.

DISCUSSION

In this report, we introduce APFBzcholine as a photoreactive nAChR partial agonist and identify the agonist binding site amino acids it photolabels in the *Torpedo* nAChR when bound at equilibrium. The photoreactive azide in APFBzcholine is incorporated at the same para position of the benzene ring as the photoreactive groups in the previously characterized Bz_2choline (*14*) and TDBzcholine (*15*), compounds we previously classified as nAChR competitive antagonists since they elicited no detectable current responses from *Torpedo* nAChRs expressed in *Xenopus* oocytes. For nAChRs expressed in oocytes and assayed by a two-electrode voltage clamp, APFBzcholine is a low-efficacy agonist, producing for embryonic mouse and *Torpedo* nAChRs maximal responses that were 0.3 and 0.1% of that of ACh, respectively. We found that Bz_2choline and TDBzcholine are also low-efficacy partial agonists for mouse nAChRs expresssed in oocytes, producing maximal responses that are 0.1% of that of ACh (data not shown). It is thus likely that they also activate *Torpedo* nAChRs, but at such low efficacy that responses are not detected under our standard assay conditions.

[^{3}H]APFBzcholine bound with high affinity ($K_{eq} = 4\ \mu$M) to the agonist binding sites in the *Torpedo* nAChR in the desensitized state and, based upon the inhibition of [^{3}H]PCP binding ($IC_{50} = 850\ \mu$M), with 100-fold lower affinity to the nAChR ion channel domain. Since azidoperfluorobenzoate esters have an absorption maximum at ~270 nm with no additional peak at longer wavelengths, we compared patterns of nAChR photolabeling after illumination at short and long UV wavelengths. Irradiation at 365 nm resulted in agonist-inhibitable labeling only in the γ and δ subunits, while 254 nm irradiation resulted in agonist-inhibitable labeling at equal efficiency in the α, γ, and δ subunits. For irradiation at 365 nm, ~2−3% of γ and δ subunits were specifically photolabeled, which is close to the ~6−8% labeling of those subunits seen for [^{3}H]Bz_2choline under similar labeling conditions (i.e., binding site ocupancy, lamp, and irradiation time) (*14*). For irradiation at 254 nm, the 5−6% level of specific labeling of the α, γ, and δ subunits by [^{3}H]APFBzcholine is more than 10-fold higher than the level of [^{3}H]nicotine photolabeling of α (0.5%) or γ (0.1%) subunits under similar labeling conditions (*31*). The fact that α subunit labeling was seen only with 254 nm irradiation suggests that the photoreactive intermediates responsible for photolabeling may differ for 254 and 365 nm irradiation. Possible explanations will be discussed later after consideration of the binding site amino acids photolabeled at 254 nm in terms of a homology model of the nAChR agonist binding site.

Proposed Orientation of APFBzcholine from Photolabeling and Molecular Modeling. Irradiation at 254 nm resulted in

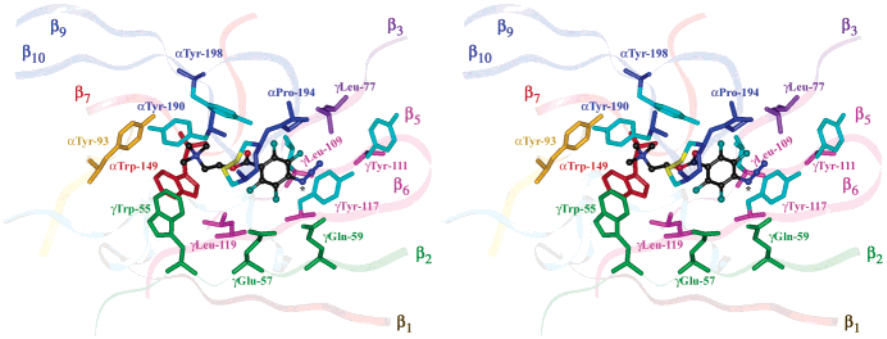

FIGURE 8: Stereoview of APFBzcholine docked within a homology model of the *Torpedo* nAChR agonist site. A homology model of the *Torpedo* nAChR extracellular region was constructed from the snail AChBP structure (*26*), and APFBzcholine was docked within the agonist binding site located at the α−γ subunit interface as described in Experimental Procedures. APFBzcholine is shown as a ball-and-stick structure with atom types colored as follows: black for carbon, blue for nitrogen, red for oxygen, and teal for fluorine. Residues near the docked APFBzcholine in the nAChR model are shown in stick representation with their colors corresponding to the different agonist site segments (ribbons): segment A in gold, segment B in red, segment C in blue, segment D in green, and segment E in magenta. β strand numbering follows that of the AChBP structure. The side chains of amino acids photolabeled by APFBzcholine are colored cyan, and the sulfur atoms of the αCys-192−αCys-193 disulfide are colored yellow. The asterisk identifies the nitrogen that forms a nitrene upon photoactivation.

specific labeling of γLeu-109/δLeu-111 at ~10 cpm/pmol, which indicates labeling of those amino acids at ~4% efficiency. In addition, γTyr-111 and γTyr-117 were labeled at ~1% efficiency. No labeling was detected in γTrp-55, the amino acid in the γ subunit labeled most efficiently by [^{3}H]nicotine (*12*) or [^{3}H]dTC (*11*). Within the α subunit, >90% of specific labeling was restricted to a 20 kDa fragment containing the amino acids of binding site segment C (α190−198), within which αTyr-198 was labeled most efficiently (~20 cpm/pmol), with αTyr-190, αCys-192, and αCys-193 labeled less efficiently. When APFBzcholine is docked in the agonist binding site at the interface of α and γ subunits in a nAChR homology model (*27*) based upon the structure of the AChBP (*26*), the quaternary ammonium occupies the core aromatic binding pocket made up of the side chains from αTyr-93, αTrp-149, αTyr-190, αTyr-198, and γTrp-55, and the substituted benzoic acid is oriented toward amino acids in segment E (β5′ and β6) and segment D (β2) (Figure 8). In the model, the azide is oriented toward γTyr-117, with the reactive nitrogen 4 Å from γTyr-117, 6 Å from γLeu-109, and 8 Å from γTyr-111. The closest amino acid side chain in the α subunit is αPro-194 at a distance of 5 Å, while αTyr-198 is at a distance of 8 Å. The labeling of γLeu-109, γTyr-111, or γTyr-117 indicates that the general orientation of APFBzcholine in the binding site is similar to that of Bz_2choline or TDBzcholine. For this orientation, the efficient photolabeling of αTyr-198 is not expected for a nitrene-based reaction mechanism, and the labeling may be evidence that APFBzcholine can also bind to the nAChR in an alternative orientation, with the aryl azide oriented more toward the core aromatic binding pocket.

Implications for nAChR Activation. For APFBzcholine, Bz_2choline, and TDBzcholine, photoactivation generates reactive intermediates at the para position of the benzene ring 10 Å from the quaternary ammonium. The efficient photolabeling of γLeu-109/δLeu-111 by each ligand establishes the proximity of the para substituents with residues in the γ (or δ) subunit, and benzoylcholine will likely be bound in a similar orientation. The photolabeling results predict that interactions with amino acids in the γ or δ subunit make important contributions to the energetics of ligand binding, a prediction that can be tested by appropriate mutational analyses. The photolabeling results, in conjunction with the decreasing agonist efficacy (Bzcholine > APFBzcholine > Bz_2choline) seen for para substituents of increasing size, suggest that it is the enhanced interaction with the γ or δ subunit that reduces efficacy.

In the structures of the transmitter binding sites in AChBP (*5*) and in the *Torpedo* nAChR in the absence of agonist (closed state) (*30*), the amino acids of binding site segments D and E from the γ and δ subunits lie on the surface of a β sheet that exists as a rigid surface of similar structure. The transmitter binding site in the *Torpedo* nAChR in the closed state differs from that of the AChBP and our nAChR homology model primarily because of a repositioning of β strands 9 and 10 that results in a disruption of the structure of the core aromatic box formed by nAChR αTyr-93, αTrp-149, αTyr-190, αTyr-198, and γTrp-55/δTrp-57. For the benzoylcholine esters, energetic interactions of the aromatic with amino acids in the γ and δ subunits will be similar in the closed and open states, and interactions of the quaternary ammonium with the "core" aromatic side chains in the open state will make up a smaller contribution to the total energetics of binding than for high-efficacy agonists such as tetramethylammonium and ACh (*32*). Presumably, benzoylcholine and its photoreactive derivatives are only low-efficacy agonists because state-independent interactions with the γ and δ subunits determine the position of the quaternary ammonium in the binding site, preventing its optimal interactions with the aromatic amino acid side chains that form the agonist binding pocket in the open state.

Mechanism of Photoincorporation of Perfluoroaryl Azide into Proteins. APFBzcholine photolabeling of an aliphatic side chain can occur only if singlet nitrene reactivity dominates, rather than a triplet nitrene (for which insertion is unfavorable) or a ring-expanded didehydroazepine (which would favor reaction with nucleophilic side chains) (*33*). While singlet nitrene reactivity is predicted from model system studies (*18*, *19*), to our knowledge there have been no reports of specific amino acids photolabeled by any perfluoroaryl azide photoafinity probe. The efficient labeling of γLeu-109/δLeu-111 by [^{3}H]APFBzcholine establishes that the perfluoroaryl azide can generate a photoreactive intermediate, presumably the singlet nitrene, that inserts ef-

ficiently into aliphatic side chains. On the basis of the labeling seen at the level of the intact subunits, agonist-inhibitable labeling in the α subunit was seen only for 254 nm irradiation, while specific labeling of the γ and δ subunits was seen at 365 and 254 nm. Since within the α subunit αTyr-198 was labeled most efficiently, further studies are required to determine whether the labeling of γTyr-111/γTyr-117 seen at 254 nm would also be seen at 365 nm. Irradiation at 254 nm can also produce photoreactive tyrosyl intermediates and cysteinyl radical, which might contribute to some of the observed labeling.

The results presented here establish that perfluoroaryl azides can be efficiently photoincorporated into aliphatic as well as nucleophilic side chains. APFBzcholine is itself a nAChR partial agonist characterized by very low efficacy, but in the future, it will be important to determine whether other quaternary ammonium perfluoroaryl azides function as photoreactive, high-efficacy nAChR agonists.

REFERENCES

1. Corringer, P.-J., Le Novere, N., and Changeux, J.-P. (2000) Nicotinic receptors at the amino acid level, *Annu. Rev. Pharmacol. Toxicol. 40*, 431−458.
2. Karlin, A. (2002) Emerging structure of the nicotinic acetylcholine receptors, *Nat. Rev. Neurosci. 3*, 102−114.
3. Sine, S. M. (2002) The nicotinic receptor ligand binding domain, *J. Neurobiol. 53*, 431−446.
4. Sixma, T. K., and Smit, A. B. (2003) Acetylcholine binding protein (AChBP): A secreted glial protein that provides a high-resolution model for the extracellular domain of pentameric ligand-gated ion channels, *Annu. Rev. Biophys. Biomol. Struct. 32*, 311−334.
5. Celie, P. H. N., van Rossum-Fikkert, S. E., van Dijk, W. J., Brejc, K., Smit, A. B., and Sixma, T. K. (2004) Nicotinic and carbamylcholine binding to nicotinic acetylcholine receptors as studied in AChBP crystal structures, *Neuron 41*, 907−914.
6. Fu, D. X., and Sine, S. M. (1994) Competitive antagonists bridge the α−γ subunit interface of the acetylcholine receptor through quaternary ammonium−aromatic interactions, *J. Biol. Chem. 269*, 26152−26157.
7. Willcockson, I. U., Hong, A., Whisenant, R. P., Edwards, J. B., Wang, H., Sarkar, H. K., and Pedersen, S. E. (2002) Orientation of δ-tubocurarine in the muscle nicotinic acetylcholine receptor-binding site, *J. Biol. Chem. 277*, 42249−42258.
8. Wang, H. L., Gao, F., Bren, N., and Sine, S. M. (2003) Curariform antagonists bind in different orientations to the nicotinic receptor ligand binding domain, *J. Biol. Chem. 278*, 32284−32291.
9. Zhong, W. G., Gallivan, J. P., Zhang, Y. N., Li, L. T., Lester, H. A., and Dougherty, D. A. (1998) From ab initio quantum mechanics to molecular neurobiology: A cation-π binding site in the nicotinic receptor, *Proc. Natl. Acad. Sci. U.S.A. 95*, 12088−12093.
10. Beene, D. L., Brandt, G. S., Zhong, W., Zacharias, N. M., Lester, H. A., and Dougherty, D. A. (2002) Cation-π interactions in ligand recognition by serotonergic ($5\text{-}HT_{3A}$) and nicotinic acetylcholine receptors: The anomalous binding properties of nicotine, *Biochemistry 41*, 10262−10269.
11. Chiara, D. C., and Cohen, J. B. (1997) Identification of Amino Acids Contributing to High and Low Affinity d-Tubocurarine Sites in the *Torpedo* Nicotinic Acetylcholine Receptor, *J. Biol. Chem. 272*, 32940−32950.
12. Chiara, D. C., Middleton, R. E., and Cohen, J. B. (1998) Identification of tryptophan 55 as the primary site of [^{3}H]nicotine photoincorporation in the γ-subunit of the *Torpedo* nicotinic acetylcholine receptor, *FEBS Lett. 423*, 223−226.
13. Grutter, T., EhretSabatier, L., Kotzybahibert, F., and Goeldner, M. (2000) Photoaffinity labeling of *Torpedo* nicotinic receptor with the agonist [H-3]DCTA: Identification of amino acid residues which contribute to the binding of the ester moiety of acetylcholine, *Biochemistry 39*, 3034−3043.
14. Wang, D., Chiara, D. C., Xie, Y., and Cohen, J. B. (2000) Probing the structure of the nicotinic acetylcholine receptor with 4-benzoylbenzoylcholine, a novel photoaffinity competitive antagonist, *J. Biol. Chem. 275*, 28666−28674.
15. Chiara, D. C., Trinidad, J. C., Wang, D., Ziebell, M. R., Sullivan, D., and Cohen, J. B. (2003) Identification of amino acids in the nicotinic acetylcholine receptor agonist binding site and ion channel photolabeled by 4-[(3-trifluoromethyl)-3*H*-diazirin-3-yl]-benzoyllcholine, a novel photoaffinity antagonist, *Biochemistry 42*, 271−283.
16. Ormerod, W. E. (1956) The pharmacology of benzoylcholine derivatives and the nature of carbonyl receptors, *Br. J. Pharmacol. 11*, 267−272.
17. Keana, J. F. W., and Cai, S. X. (1990) New reagents for photoaffinity labeling: Synthesis and photolysis of functionalized perfluorophenyl azides, *J. Org. Chem. 55*, 3640−3647.
18. Schnapp, K. A., and Platz, M. S. (1993) A laser flash photolysis study of di-, tri- and tetrafluorinated phenylnitrenes; implications for photoaffinity labeling, *Bioconjugate Chem. 4*, 178−183.
19. Kotzyba-Hibert, F., Kapfer, I., and Goeldner, M. (1995) Recent trends in photoaffinity labeling, *Angew. Chem., Int. Ed. 34*, 1296−1312.
20. Pinney, K. G., Carlson, K. E., Katzenellenbogen, B. S., and Katzenellenbogen, J. A. (1991) Efficient and selective photoaffinity labeling of the estrogen receptor using two nonsteroidal ligands that embody aryl azide or tetrafluoroaryl azide photoreactive functions, *Biochemistry 30*, 2421−2431.
21. Pandurangi, R. S., Karra, S. R., Kuntz, R. R., and Volkert, W. A. (1997) Recent trends in the evaluation of photochemical insertion characteristics of heterobifunctional perfluoroaryl azide chelating agents: Biochemical implications in nuclear medicine, *Photochem. Photobiol. 65*, 208−221.
22. Pedersen, S. E., Dreyer, E. B., and Cohen, J. B. (1986) Location of ligand binding sites on the nicotinic acetylcholine receptor α-subunit, *J. Biol. Chem. 261*, 13735−13743.
23. White, B. H., Howard, S., Cohen, S. G., and Cohen, J. B. (1991) The hydrophobic photoreagent 3-(trifluoromethyl)-3-(m-[^{125}I]-iodophenyl)diazirine is a novel noncompetitive antagonist of the nicotinic acetylcholine receptor, *J. Biol. Chem. 266*, 21595−21607.
24. Boyd, N. D., and Cohen, J. B. (1984) Desensitization of membrane-bound *Torpedo* acetylcholine receptor by amine noncompetitive antagonists and aliphatic alcohols: Studies of [^{3}H]-acetylcholine binding and $^{22}Na^+$ ion fluxes, *Biochemistry 23*, 4023−4033.
25. White, B. H., and Cohen, J. B. (1988) Photolabeling of membrane-bound *Torpedo* nicotinic acetylcholine receptor with the hydrophobic probe 3-trifluoromethyl-3-(m-[^{125}I]iodophenyl)diazirine, *Biochemistry 27*, 8741−8751.
26. Brejc, K., van Dijk, W. J., Klaassen, R., Schuurmans, M., van der Oost, J., Smit, A. B., and Sixma, T. K. (2001) Crystal structure of AChBP reveals the ligand-binding domain of nicotinic receptors, *Nature 411*, 269−276.
27. Sullivan, D., Chiara, D. C., and Cohen, J. B. (2002) Mapping the agonist binding site of the nicotinic acetylcholine receptor by cysteine scanning mutagenesis: Antagonist footprint and secondary structure prediction, *Mol. Pharmacol. 61*, 463−472.
28. Pedersen, S. E., and Cohen, J. B. (1990) d-Tubocurarine binding sites are located at α−γ and α−δ subunit interfaces of the nicotinic acetylcholine receptor, *Proc. Natl. Acad. Sci. U.S.A. 87*, 2785−2789.
29. Oswald, R. E., Heidmann, T., and Changeux, J.-P. (1983) Multiple affinity sites for noncompetitive blockers revealed by [^{3}H]phencyclidine binding to acetylcholine receptor rich membrane fragments from *Torpedo marmorata*, *Biochemistry 22*, 3128−3136.
30. Unwin, N. (2005) Refined structure of the nicotinic acetylcholine receptor at 4 Å resolution, *J. Mol. Biol. 346*, 967−989.
31. Middleton, R. E., and Cohen, J. B. (1991) Mapping of the acetylcholine binding site of the nicotinic acetylcholine receptor: [^{3}H]Nicotine as an agonist photoaffinity label, *Biochemistry 30*, 6987−6997.
32. Akk, G., and Auerbach, A. (1996) Inorganic, monovalent cations compete with agonists for the transmitter binding site of nicotinic acetylcholine receptors, *Biophys. J. 70*, 2652−2658.
33. Bayley, H. (1983) *Photoregenerated Reagents in Biochemistry and Molecular Biology*, Elsevier, Amsterdam.

BI051209Y